

# Propulsive cell entry diverts pathogens from immune degradation by remodeling the phagocytic synapse

Zihan Zhang<sup>a</sup> , Thomas K. Gaetjens<sup>b</sup> , Jin Ou<sup>a</sup> , Qiong Zhou<sup>a</sup>, Yangi Yu<sup>a</sup>, D. Paul Mallory<sup>a</sup>, Steven M. Abel<sup>b</sup> , and Yan Yu<sup>a</sup>. 1

Edited by David M. Underhill, Cedars Sinai Medical Center, Los Angeles, CA; received May 1, 2023; accepted October 5, 2023 by Editorial Board Member Arthur Weiss

Phagocytosis is a critical immune function for infection control and tissue homeostasis. During phagocytosis, pathogens are internalized and degraded in phagolysosomes. For pathogens that evade immune degradation, the prevailing view is that virulence factors are required to disrupt the biogenesis of phagolysosomes. In contrast, we present here that physical forces from motile pathogens during cell entry divert them away from the canonical degradative pathway. This altered fate begins with the force-induced remodeling of the phagocytic synapse formation. We used the parasite Toxoplasma gondii as a model because live *Toxoplasma* actively invades host cells using gliding motility. To differentiate the effects of physical forces from virulence factors in phagocytosis, we employed magnetic forces to induce propulsive entry of inactivated *Toxoplasma* into macrophages. Experiments and computer simulations show that large propulsive forces hinder productive activation of receptors by preventing their spatial segregation from phosphatases at the phagocytic synapse. Consequently, the inactivated parasites are engulfed into vacuoles that fail to mature into degradative units, similar to the live motile parasite's intracellular pathway. Using yeast cells and opsonized beads, we confirmed that this mechanism is general, not specific to the parasite used. These results reveal new aspects of immune evasion by demonstrating how physical forces during active cell entry, independent of virulence factors, enable pathogens to circumvent phagolysosomal degradation.

propulsion force | magnetic manipulation | phagocytic synapse | immune evasion | phagosome maturation

Phagocytosis is a vital process for innate immune cells to ingest and degrade invading pathogens. It starts with immune cell receptors recognizing the pathogen. This leads to the formation of the phagocytic synapse, where activated receptors and other signaling proteins at the pathogen-host contact site reorganize spatially to form a microscale pattern (1–3). Signaling from activated receptors then triggers actin remodeling in immune cells to engulf the pathogen into a membrane-bounded compartment (phagosome). Nascent phagosomes mature into degradative phagolysosomes through sequential steps, including acidification in the lumen (4), fusion with endosomes and lysosomes (5, 6), and acquisition of hydrolytic enzymes for content digestion (7–9). This eventually leads to the elimination of the pathogen.

Many pathogens have evolved diverse strategies to evade immune cell surveillance and degradation. Some, like *Bacillus subtilis*, avoid internalization by injecting virulence factors into host cells to deactivate phagocytosis (10-13) or modifying their cell envelopes to avoid recognition (14, 15). Some other pathogens like Mycobacterium tuberculosis and Streptococcus pyogenes are internalized but survive intracellularly by circumventing the phagolysosomal degradation pathway. Their known mechanisms involve using virulence effectors to inhibit phagosome acidification or phagosome-lysosome fusion (16-19). It was believed that pathogens, once inside the host, primarily rely on virulence factors to evade immune degradation. However, given that pathogen motility was shown to be important for invasion (20, 21), one must wonder if it might also contribute to the immune evasion of pathogens. Notably, current research on pathogen motility has predominantly focused on its importance in the initial pathogen-cell contact, before host entry. For example, Legionella was found to use flagella to promote its encounter with the host cell (22). Apicomplexans, causing diseases like malaria, use gliding motility (23–25) to promote pathogen binding to host cells (22, 26) and active penetration of the host cell membrane (27, 28). Despite those findings, it remains unclear how pathogen motility impacts their intracellular fate after they enter the cell.

To address this question, here we investigate how physical forces, as expected from motile pathogens, might impact their intracellular trafficking. Our study uses the protozoan parasite Toxoplasma gondii as the pathogen model, complemented by using yeast and opsonized beads for generality confirmation. Toxoplasma is an intracellular pathogen that causes

## **Significance**

Immune cells control infections by ingesting and degrading pathogens. However, some pathogens escape this defense mechanism to multiply inside host cells. While known evasion mechanisms involve virulence factors, many pathogens are mobile during invasion. How might the physical forces exerted by motile pathogens affect their degradative fate within the host? Here, we magnetically apply propulsive forces during cell entry of the parasite Toxoplasma and monitor its intracellular trafficking. By combining experiments and simulations, we demonstrate that propulsive forces from active cell entry hinder the phagocytic synapse assembly, diverting pathogens into a nondegradative trafficking pathway. This mechanism elucidates the contribution of physical forces in immune evasion and underscores the importance of targeting pathogen movement to combat intracellular infections.

Author contributions: Z.Z. and Y.Y. designed research; Z.Z., T.K.G., J.O., Q.Z., Y.-q.Y., D.P.M., and S.M.A. performed research; Y.-q.Y. contributed new reagents/analytic tools; Z.Z., T.K.G., J.O., Q.Z., and S.M.A. analyzed data; and Z.Z., T.K.G., S.M.A., and Y.Y. wrote the paper.

The authors declare no competing interest.

This article is a PNAS Direct Submission. D.M.U. is a guest editor invited by the Editorial Board.

Copyright © 2023 the Author(s). Published by PNAS. This article is distributed under Creative Commons Attribution-NonCommercial-NoDerivatives License 4.0

<sup>1</sup>To whom correspondence may be addressed. Email:

This article contains supporting information online at https://www.pnas.org/lookup/suppl/doi:10.1073/pnas. 2306788120/-/DCSupplemental.

Published November 30, 2023.

congenital disorders and complications in immunocompromised individuals. Toxoplasma's gliding motility, powered by its cytoskeleton and myosin motors, is crucial for infection (27, 28), especially for its active penetration of the host cell membrane (29–31). After internalization, Toxoplasma resides in parasitophorous vacuoles that do not acidify (32) or fuse with lysosomes (33, 34). The lack of degradative functions of these vacuoles allows the parasite to survive and replicate inside. It was proposed that *Toxoplasma* during active invasion releases effector proteins that block the residing vacuoles from fusing with lysosomes (33, 35–37). However, like other motile pathogens, it remains unclear whether and how the propulsive force from active penetration might help the parasite's trafficking into the nondegradative pathway.

A major challenge in addressing this question is differentiating the effects of physical forces from the biochemical effects of virulence systems that are often coordinately regulated with the motility apparatus (20). To study the role of pathogen motility in infection, one widely used approach is to generate motility mutants. However, this approach has drawbacks. Motility mutants can still have residual motility, and the same mutation causing motility deficit could also disrupt other protein functions involved in virulence systems. Such drawbacks possibly led to discrepancies between previous studies (26, 38).

In this study, we developed a method to examine the impact of propulsive cell entry by using magnetic manipulation during pathogen internalization. Using Toxoplasma as the model pathogen, we attached magnetic nanoparticles to inactivated parasites, rendering them magnetically responsive. We propelled these parasites into macrophage cells while monitoring their intracellular fate. Normally, inactivated *Toxoplasma* is degraded in phagolysosomes. However, when induced to actively penetrate the macrophage cells, just like live parasites, can physical force alone alter their phagocytic fate? We show that the propulsive force applied during cell entry diverts inactivated parasites into vacuoles lacking degradative capacity, similar to the live parasite's intracellular pathway. This altered fate results from force-induced disruption of the phagocytic synapse formation, where large propulsive forces prevent the productive activation of receptors by hindering their spatial segregation from phosphatases at the parasite-cell contact

area. We extended the findings to Saccharomyces cerevisiae yeast and opsonized beads, confirming that this effect of physical forces is general regardless of the type of phagocytic targets.

#### Results

Live Toxoplasma Resides in Vacuoles Lacking Degradative Functions, but Heat-Killed Toxoplasma is Degraded in Phagolysosomes. It has been shown that Toxoplasma, upon penetrating the host cell membrane, enters vacuoles that fail to acidify or fuse with endocytic vesicles (32-34). To first confirm this, we added live Toxoplasma to macrophage cells (RAW 264.7 cell line) and then examined the recruitment of endocytic and lysosomal markers on the Toxoplasmacontaining vacuoles using fluorescence microscopy. These markers, including small GTPase Rab5, Rab7, and lysosome-associated membrane proteins (LAMP)1, regulate phagosome fusion with endosomes and lysosomes (Fig. 1A) (39-42), facilitating the delivery of degradative enzymes into phagosomes (7, 8, 43, 44). Consequently, the accumulation of these markers indicates the proper maturation and degradative function of phagosomes (45, 46). By imaging the recruitment of Rab5-GFP, Rab7-RFP, and LAMP1-RFP, we found negligible recruitment of any of these three markers on most vacuoles containing live Toxoplasma (expressing tubulin GFP for visualization) (Fig. 1 B–D). Only a small fraction of the vacuoles was positive for Rab5, Rab7, and LAMP1, likely because some of the *Toxoplasma* tachyzoites were dead during the isolation and purification process. We then prepared heat-killed Toxoplasma and added them to the cells. Different from live Toxoplasma, the heat-killed ones were engulfed into phagosomes that showed accumulation of all three markers, with Rab5 accumulation shortly after internalization and followed by Rab7 and LAMP1 accumulation (Fig. 1 B-D). These results confirm that live Toxoplasma resided in intracellular vacuoles that lack degradative functions, whereas heat-killed Toxoplasma was passively internalized via the canonical phagolysosomal degradative pathway. Having confirmed this result, we then asked: if the heat-killed parasite can be made to exert propulsion force during cell entry, like the live parasite does, can the physical force alter its intracellular trafficking fate?

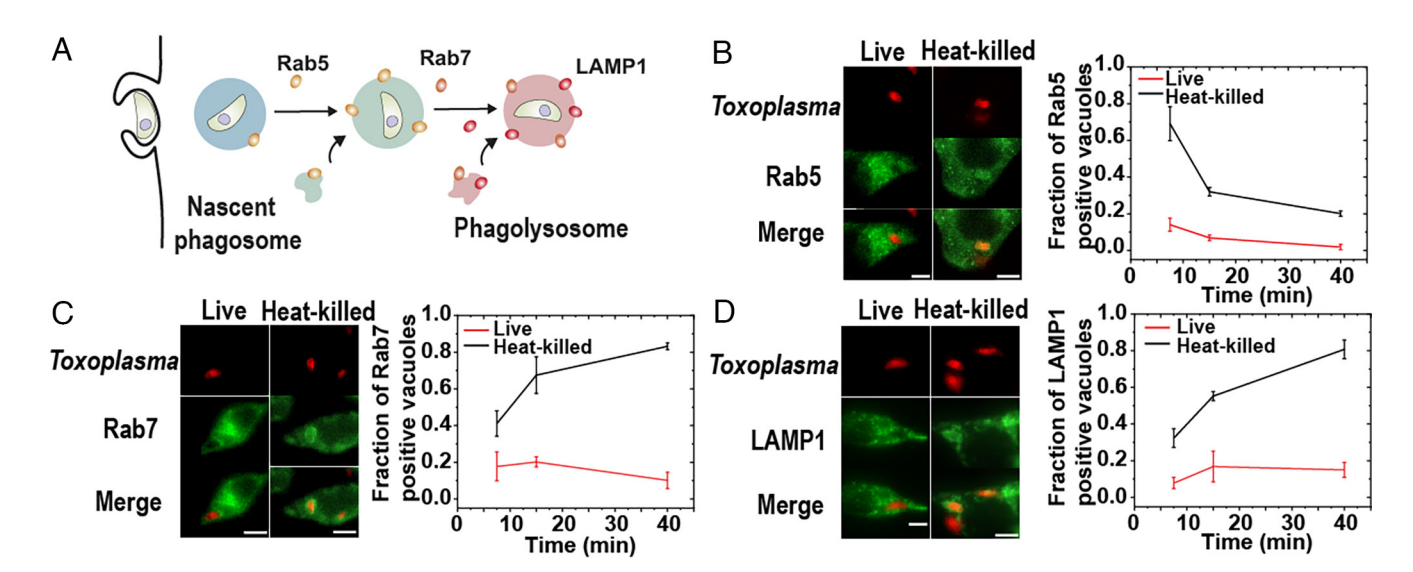


Fig. 1. Live and heat-killed Toxoplasma entered distinct intracellular trafficking pathways in RAW 264.7 cells. (A) Schematic illustration showing Rab5, Rab7, and LAMP1 recruitment during canonical phagosome maturation. (B-D) Fluorescence images and quantitative analysis of the assembly of endocytic markers Rab5, Rab7, and LAMP1 on phagosomes encapsulating heat-killed *Toxoplasma* versus vacuoles encapsulating live *Toxoplasma*. Data were obtained at 7.5 min, 15 min, and 40 min after parasites were added to cells. Error bars in line plots represent SDs from 3 independent experiments. (Scale bars, 5 µm.)

Design and Characterization of Magnetically Responsive Heat-Killed Toxoplasma. We induced the propulsive cell entry of heat-killed Toxoplasma by using a magnetic tweezers setup (SI Appendix, Fig. S1) and then simultaneously imaged their intracellular trafficking in RAW 264.7 cells (Fig. 2A). Briefly, 200-nm magnetic nanoparticles were covalently conjugated onto the surface of heat-killed Toxoplasma to render them magnetically responsive (Fig. 2A). Using fluorescent magnetic nanoparticles, we found that ≈46% of the heat-killed *Toxoplasma* tachyzoites were conjugated with magnetic nanoparticles, which we referred to as Mag-Toxoplasma for simplicity (SI Appendix, Fig. S2 A and B). Most Mag-Toxoplasma had 1 to 5 magnetic nanoparticles, as shown in scanning electron microscopy (SEM) micrographs (Fig. 2B). We selected 200-nm magnetic particles as they provide robust magnetic forces without blocking the major surface antigen (SAG-1) of Toxoplasma or hindering their host cell entry (SI Appendix, Fig. S2A). One single 200-nm magnetic nanoparticle can exert forces of 5 to 10 pN (SI Appendix, Fig. S2C), and the magnetic force decays with increased distance between the nanoparticle and the solenoid tip, consistent with theoretical predictions (47-50). We cannot establish a similar force-distance plot for heat-killed *Toxoplasma* because the movement of these irregularly shaped, deformable parasites does not follow the Stokes' equation. Nevertheless, we confirmed that the Mag-Toxoplasma are magnetically responsive by observing their faster directional movements toward the solenoid tip (SI Appendix, Fig. S3). The magnetic force on a single Mag-Toxoplasma was estimated to be around 10 to 50 pN, depending on the number of conjugated nanoparticles per parasite. This range of force is comparable to forces generated from the gliding motion of living *Toxoplasma* (51) and Mycoplasma pneumoniae on surfaces (52).

In our experiments, we first allowed the Mag-Toxoplasma to bind to the RAW 264.7 cells in a culture dish and then used the

magnetic tweezers to pull the membrane-bound Mag-Toxoplasma toward the cell center (Fig. 2 A and C). This magnetic pulling was intended to mimic the propulsion force exerted by live *Toxoplasma* during cell entry. We maintained the magnetic force after the internalization of Mag-Toxoplasma throughout the imaging process, unless otherwise specified. Under the magnetic pulling force, the Mag-Toxoplasma initially adhered to the cell membrane and then moved rapidly and directionally toward the tip of the magnetic tweezers upon internalization (Fig. 2C). Using gangliosides GM1 marker CTB-CF488 to label the cell plasma membrane, we confirmed that the Mag-Toxoplasma was internalized into membrane vacuoles marked by CTB-CF488 fluorescence (Fig. 2C). The magnitude of magnetic force we applied was suitable to allow engulfment of the heat-killed parasite without rupturing the plasma membrane.

### Heat-Killed Toxoplasma with Induced Propulsive Cell Entry Enters Vacuoles That Do Not Fuse with Endosomes or Lysosomes. We next sought to investigate whether the vacuoles containing Mag-Toxoplasma after propulsive cell entry mature into phagolysosomes. We have shown that when heat-killed Toxoplasma was internalized without magnetic force, the endocytic markers Rab5 and Rab7, and lysosomal marker LAMP1, were present on phagosomes as expected for typical phagosome maturation (Fig. 1 B-D). In live cell imaging, we observed that Rab5-GFP was recruited transiently to the phagosome membrane containing heat-killed Toxoplasma, reaching an intensity peak shortly after internalization and then gradually decreasing afterward (Fig. 2D; single phagosome data in SI Appendix, Fig. S4A). LAMP1-GFP was continuously recruited to the phagosome (Fig. 2E; single phagosome data in SI Appendix, Fig. S5A). In contrast, when magnetic force was applied during internalization, the vacuoles containing Mag-Toxoplasma showed significantly impaired recruitment of Rab5 and

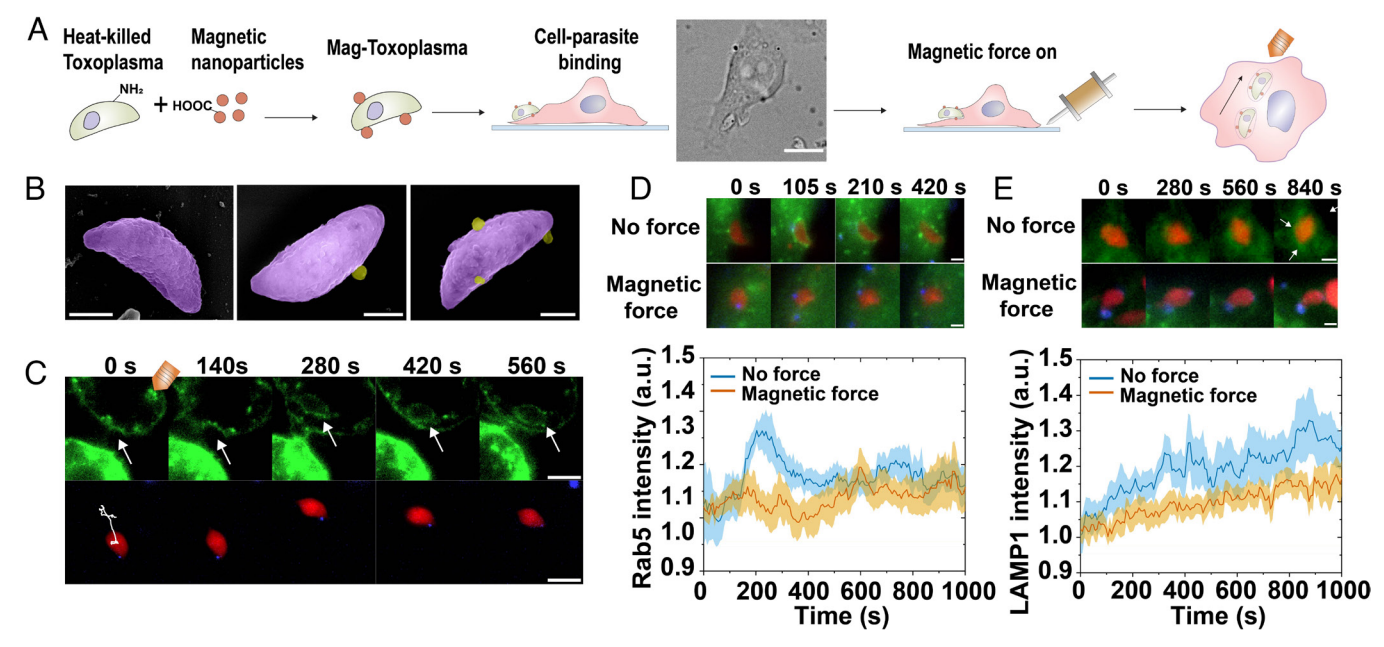


Fig. 2. Propulsion force during cell entry causes heat-killed Toxoplasma to enter vacuoles lacking endocytic markers. (4) Schematic illustration of the experiment design. (Scale bar in bright-field image, 10 µm.) (B) SEM images of Mag-Toxoplasma. Images are assigned with pseudocolors, Toxoplasma in magenta and magnetic nanoparticles in yellow. (Scale bars, 2 μm.) (C) Fluorescence images showing the cell entry of a Mag-Toxoplasma under magnetic force. Mag-Toxoplasma was labeled with Alexa 568 (shown in red), magnetic nanoparticles were labeled with CF640R (shown in blue), and macrophage cell membrane was labeled with CF488A-Cholera Toxin Subunit B (CTB) (shown in green). The white line in the first image shows the trajectory of the Mag-Toxoplasma. (Scale bars, 5 µm.) (D and E) Fluorescence images show the assembly of Rab5 (D) and LAMP1 (E) on phagosomes encapsulating heat-killed Toxoplasma with or without magnetic pulling force. Toxoplasma is shown in red, magnetic nanoparticles in blue, and Rab5-GFP and LAMP1-GFP in green. (Scale bars, 2 µm.) Line plots show the average fluorescence intensity of Rab5-GFP and LAMP1-GFP on phagosomes with or without magnetic pulling force. Line curves are averages from 13 (no force) and 15 (with magnetic force) single phagosomes. Shaded areas represent the SEM. (Scale bars, 2 μm.)

LAMP1 (Fig. 2 D and E; single phagosome data in SI Appendix, Figs. S4B and S5B). This indicates that the inactivated *Toxoplasma* with propulsive cell entry was internalized into vacuoles that fail to recruit the endocytic markers for maturation. Next, we sought to determine whether this observation is specific to Toxoplasma or it generalizes to other types of internalized particles. For simplicity, from here on, we will refer to the vacuoles formed after propulsive cell entry as phagosomes, even though they may not function as normal phagosomes.

To test the generality of our findings, we performed experiments using 1 µm magnetic beads opsonized with immunoglobulin G (IgG), which triggers Fc gamma receptor (FcγR)-mediated phagocytosis (Fig. 3A) (53, 54). The propulsive force exerted by a 1 µm magnetic bead was estimated to be about 25 pN at the beginning of magnetic manipulation and 30 pN at the end (SI Appendix, Figs. S6 and S7). We confirmed the internalization of the beads by using a trypan blue quenching assay and by directly imaging the phagosome membrane using a plasma membrane marker PM-RFP (SI Appendix, Fig. S8). Without magnetic force, Rab5-GFP was recruited and then dissociated from the bead-containing phagosomes, followed by the gradual recruitment of Rab7-GFP and LAMP1-GFP (Fig. 3 B-D and SI Appendix, Figs. S9A, S10A, and S11A). However, there was no significant recruitment of these markers to the phagosomes when magnetic force was applied. This is consistent with the results from Mag-Toxoplasma experiments.

The recruitment of Rab5, Rab7, and LAMP1 are prerequisites for phagosomes to fuse with lysosomes to acquire digestive enzymes. Therefore, we next directly quantified how propulsive force affects the phagosome fusion with lysosomes using a Förster Resonance Energy Transfer (FRET)-based assay (Fig. 3E). Details of this assay have been described in our recent study (55). Briefly, 1-µm magnetic beads were coated with streptavidin labeled with donor fluorophore Alexa 568 (referred to as FRET-MagSensors), whereas lysosomes in cells were loaded with biotinylated bovine serum albumin (BSA) that was labeled with acceptor fluorophore Alexa 647. Upon phagosome fusion with lysosomes, streptavidin-Alexa 568 on the surface of the FRET-MagSensors mixes with fragmented BSA-biotin-Alexa 647 in lysosomes, resulting in FRET signals (SI Appendix, Fig. S12A). Since each phagosome can fuse simultaneously with multiple lysosomes, the fusion events collectively resulted in a gradual decrease in donor emission (Alexa 568, ex/em: 561/586 nm) and concurrently an increase in FRET signal, which is acceptor emission under donor excitation (Alexa 647, ex/em: 561/680 nm) (SI Appendix, Fig. S12C). Therefore, the FRET ratio,  $\frac{FRET_{em}}{AF568_{em}}$ , indicates the extent of phagosome–lysosome fusion.

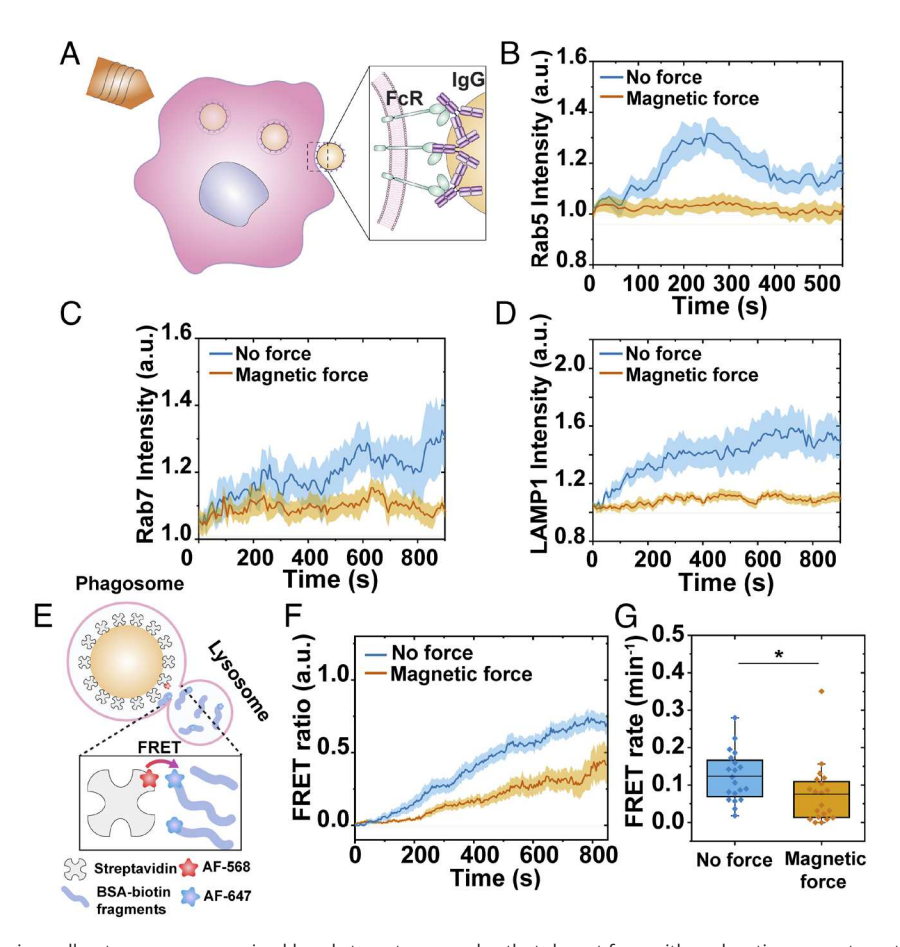


Fig. 3. Propulsion force during cell entry causes opsonized beads to enter vacuoles that do not fuse with endocytic compartments. (A) Schematic illustration of the experimental design. (*B–D*) Line plots showing the average time-dependent intensity of assembly of Rab5-GFP (no force, N = 15; with magnetic force, N = 15), Rab7-GFP (no force, N = 8; with magnetic force, N = 10), and LAMP1-GFP (no force, N = 9; with magnetic force, N = 11) on bead-containing phagosomes. Shaded areas represent the SEM. (E) Schematic illustration showing the working principle of phagosome-lysosome fusion measurements based on FRET. (F) Line plots show the average FRET ratio as a function of time with or without magnetic pulling force as indicated. The line curves are averages from N = 20 single phagosomes for each experimental condition. Shaded areas represent the SEM. (G) The box graph shows the average FRET rate under different experiment conditions as indicated. The average FRET rate is 0.12 ± 0.07 a.u. without magnetic force (N = 20) and 0.07 ± 0.08 a.u. with magnetic pulling force (N = 20). Each box plot indicates the mean (horizontal line) and the interquartile range from 25 to 75% of the corresponding dataset. Statistical significance is highlighted by P values (Student's t test) as follows: \*P < 0.05.

Without magnetic force, the FRET ratio of single phagosomes during maturation followed a sigmoidal relationship with time (Fig. 3 and SI Appendix, Fig. S12E), which is consistent with our previous finding (55). By comparison, phagosomes formed under magnetic force exhibited a significantly slower increase in FRET ratio (Fig. 3F and SI Appendix, Fig. S12 B-F). We further quantified the kinetic rate of phagosome-lysosome fusion (referred to as FRET rate) by calculating the slope of the FRET ratio increase (SI Appendix, Fig. S12E). With magnetic pulling force, phagosomes fused with lysosomes at an average rate of  $0.07 \pm 0.08$  a.u., a decrease from the average rate of  $0.12 \pm 0.07$  a.u. without magnetic force (Fig. 3G). To confirm whether the reduced fusion of phagosomes with lysosomes was caused by the propulsive force, we performed control experiments in which we pulled FRET-MagSensors during internalization but then turned off the magnetic force after bead internalization (SI Appendix, Fig. S13A). There was negligible recovery of phagosome-lysosome fusion (SI Appendix, Fig. S13B). The results altogether indicate that propulsive cell entry, induced by magnetic force, disrupts the fusion of phagosomes with endosomes and lysosomes. This is the consequence of the impaired recruitment of endocytic markers including Rab5, Rab7, and LAMP1.

Heat-Killed Toxoplasma with Induced Propulsive Cell Entry Resides in Vacuoles Lacking Acidification and Degradative Function. During normal maturation, phagosomes fuse with lysosomes to acquire proton pump vacuolar-type H+-ATPase (V-ATPase) (56, 57) and hydrolytic enzymes (7, 8, 43, 44). The proton pumps maintain an acidic lumen environment that is required for content degradation (7, 58-60). With the observation that both Mag-Toxoplasma and beads under magnetic force were internalized into phagosomes that failed to fuse with lysosomes,

we then examined whether those phagosomes lost their capacity to acidify and degrade. To monitor the acidification of the phagosomes, we covalently conjugated a pH-sensitive dye, pHrodo Red, on the surface of the Mag-Toxoplasma (Fig. 4A). All parasites were labeled with pHrodo Red (SI Appendix, Fig. S2 A and D), and the dye labeling did not block the major SAG-1 from binding to its antibody (SI Appendix, Fig. S2E). The fluorescence intensity of pHrodo Red ( $I_{pHrodo}$ ) of single Mag-Toxoplasma increased linearly as the buffer pH decreased (average data in SI Appendix, Fig. S14A; single Mag-Toxoplasma plots in SI Appendix, Fig. S14B).

Without magnetic force, phagosomes containing Mag-Toxoplasma acidified rapidly after internalization and the acidity eventually reached a plateau around pH 4.5 (Fig. 4B and SI Appendix, Fig. S15 A-C). This three-stage acidification profile is consistent with our previous observations of phagosome acidification using synthetic beads (55, 59). We obtained the initial and final pH, and the rate of acidification, of single phagosomes by fitting their pH vs. time plots with a sigmoidal-Boltzmann function (Fig. 4B):

$$pH = pH_{final} + \frac{pH_{initial} - pH_{final}}{1 + \exp(\frac{t - t_0}{dt})}.$$

We found that the application of propulsive force on Mag-Toxoplasma during internalization impaired phagosome acidification (Fig. 4 C-E; single phagosome data in SI Appendix, Fig. S15 *D–F*). Phagosomes formed under magnetic pulling force acidified more slowly (0.44 ± 0.46 pH unit/min) and reached higher final pH  $(6.3 \pm 0.8)$  than normal phagosomes without force applied (0.85 ± 0.53 pH unit/min, final pH 4.8 ± 0.6) (Fig. 4 D and E). The impairment of phagosome acidification was similar for Mag-Toxoplasma conjugated with a varying number of magnetic nanoparticles (SI Appendix, Fig. S16), suggesting that the extent of

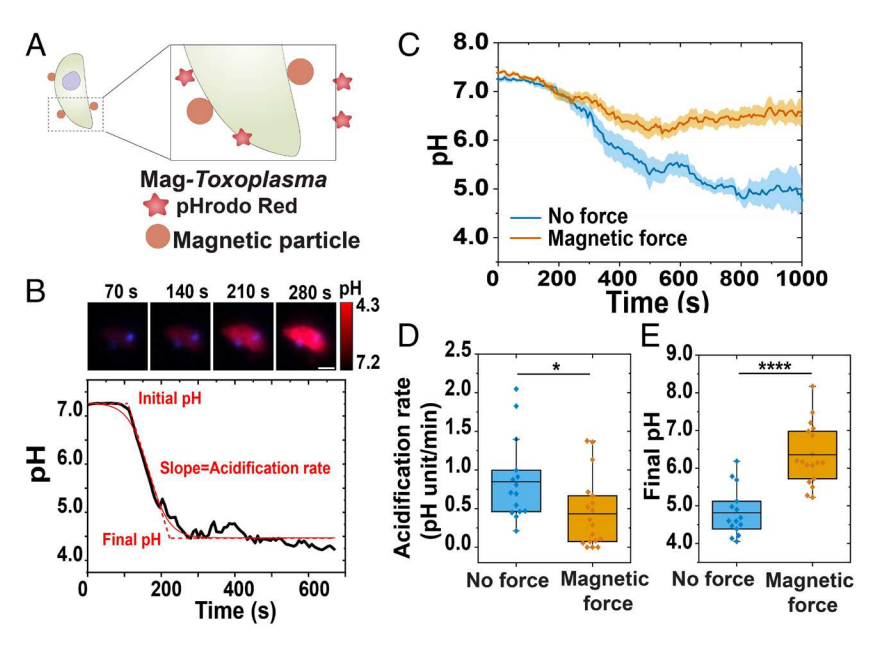


Fig. 4. Propulsion force during cell entry causes heat-killed Toxoplasma to enter vacuoles lacking acidification and degradative function. (A) Schematic illustration showing the surface functionalization of pH-sensitive Mag-Toxoplasma. (B) Fluorescence images and line curves showing the pH change of a representative Mag-Toxoplasma-containing phagosome as a function of time without magnetic manipulation. Mag-Toxoplasma is shown in red and CF-640R labeled magnetic nanoparticles in blue. (Scale bar, 2 μm.) The pH-time line plot is fitted with sigmoidal-Boltzmann function (red solid line) to determine the initial pH, final pH, and acidification rate. The red dotted line indicates the determination of slope. (Scale bar, 2 µm.) (C) Line plots showing the average heat-killed Toxoplasma containing-phagosome pH as a function of time without and with magnetic force applied. The line curves are averages from 15 (no force) and 18 (with magnetic force) individual phagosomes. Shaded areas represent the SEM. (D) Box graph showing the average acidification rate of individual Mag-Toxoplasma-containing vacuoles with or without magnetic force. The average acidification rate is  $0.85 \pm 0.53$  pH unit/min without magnetic manipulation (N = 15) and  $0.44 \pm 0.46$ pH unit/min with magnetic pulling (N = 18). (E) Box graph showing the average phagosome final pH under different experiment conditions as indicated. The average final pH is  $4.8 \pm 0.6$  without magnetic manipulation (N = 15) and E), each box plot indicates the mean (horizontal line) and the interquartile range from 25 to 75% of the corresponding dataset. Statistical significance is highlighted by P values (Student's t test) as follows: \*\*\*\*P < 0.0001 and \*P < 0.05.

disruption in phagosome maturation is not proportional to the force magnitude within the range studied here. Further, the phagosomes did not resume normal acidification when the magnetic force was turned off (SI Appendix, Fig. S17), suggesting that the effect of forces transiently applied at earlier times can impact the function of phagosomes at later times.

We confirmed that the force-induced impairment of phagosome acidification is not specific to Toxoplasma, by using magnetically responsive S. cerevisiae yeast (Mag-Yeast) (SI Appendix, Fig. S18). Yeast cells bind to Dectin-1, Toll-like receptor 2, and possibly other receptors, on RAW264.7 cells expressing GFP-Dectin-1. Similarly, the application of magnetic force diminished acidification of the yeast-containing phagosomes, as it did for the Mag-Toxoplasma.

To further test the generality of this observation, we performed experiments using pH-responsive magnetic beads (referred to as pH-MagSensors). We first biotinylated 1-µm magnetic beads, then conjugated them with a mixture of pHrodo Red-labeled streptavidin and CF640R-labeled streptavidin, and finally coated the beads with IgG via physical adsorption (Fig. 5A), following a protocol we reported previously (55). The pHrodo Red dye is the pH indicator, whereas the pH-insensitive CF640R dye is the reference. Their ratiometric fluorescence  $(I_{pHrodo}/I_{ref})$  increases linearly with decreased pH in aqueous buffers (SI Appendix, Fig. S19A) and inside phagosomes in cells (SI Appendix, Fig. S19B). As with the Mag-Toxoplasma results, magnetic force applied during the internalization of beads caused a higher final pH and the slower

acidification of phagosomes (Fig. 5 B-D; single phagosome plots in SI Appendix, Fig. S20).

We next quantified proteolytic activity of phagosomes. In these experiments, we conjugated biotinylated magnetic beads (1 µm) with CF640R-labeled streptavidin and then coated them with IgG and fluorogenic peptide Z-FR-R110 [Rhodamine 110, bis-(N-CBZ-L-phenylalanyl-L-arginine amide) dihydrochloride] (Fig. 5A). The Z-FR-R110 peptide is a substrate for cysteine proteases that degrade cargos in phagosomes (61, 62). Upon cleavage of the peptide bonds, the Rhodamine 110 dye "caged" in this fluorogenic peptide is released, resulting in strong fluorescence emission (Fig. 5E). We referred to these magnetic beads as proteolysis-MagSensors. Without magnetic force, the Rhodamine 110 intensity remained low for a few minutes after internalization, but increased rapidly afterward (Fig. 5F and SI Appendix, Fig. S21A). This late start of proteolysis is because activation of the proteases requires acidic pH in the phagosome lumen (59, 63). However, when magnetic force was applied, proteolytic activity in phagosomes was significantly impaired, as evidenced by the low level of Rhodamine 110 intensity (Fig. 5F and SI Appendix, Fig. S21B). The results from phagosome acidification and proteolysis both demonstrate that the degradative function of phagosomes was compromised by the propulsive force during internalization.

Propulsive Force Alters Protein Spatial Organization at the Phagocytic Synapse. After elucidating how propulsive cell entry perturbs phagosome maturation, we next sought to identify the cause of this disruptive effect. When microbes are phagocytosed,

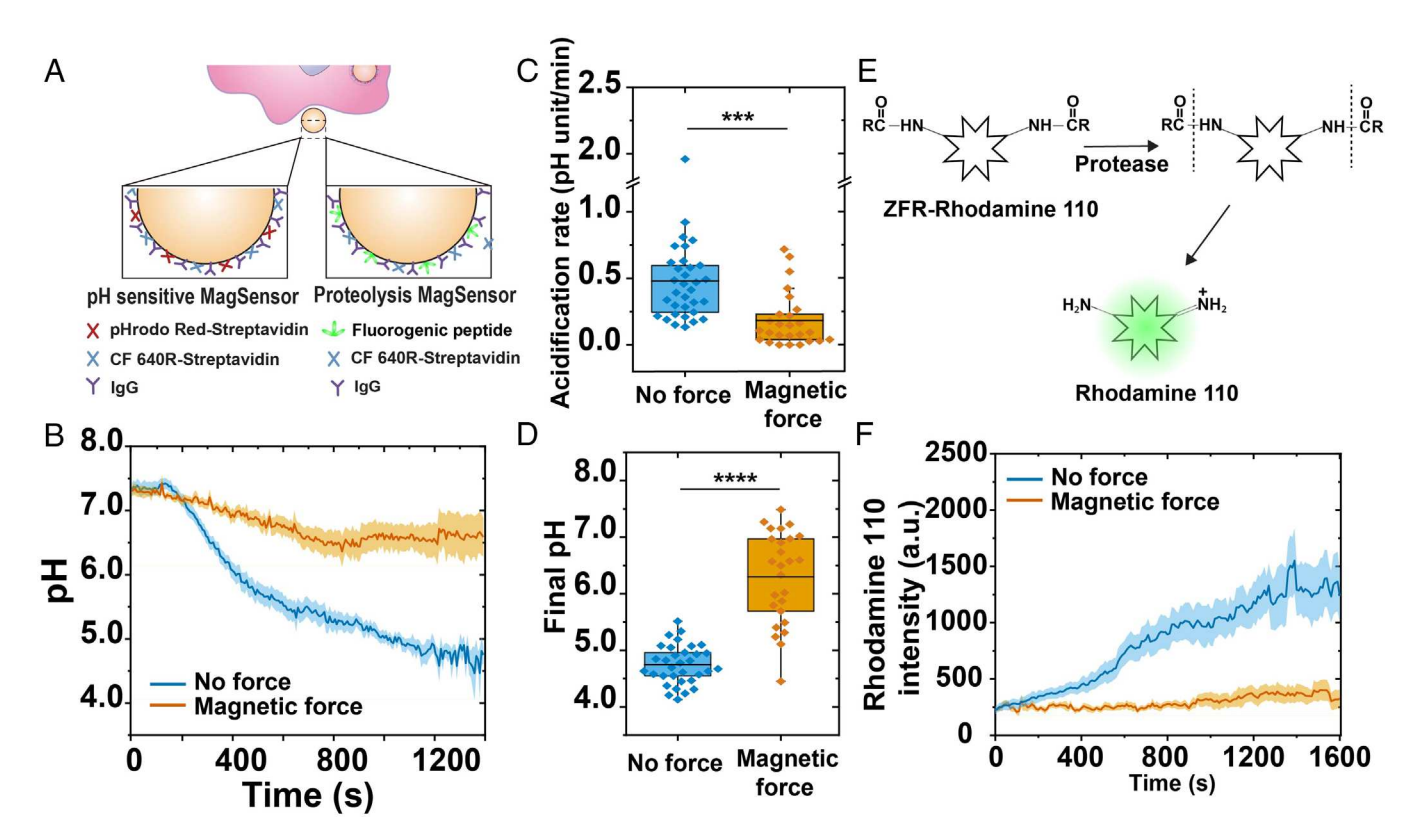


Fig. 5. Propulsion force during cell entry causes opsonized beads to enter vacuoles lacking acidification and degradative function. (A) Schematic illustration showing the design of pH-sensitive MagSensor (pH-MagSensor) and proteolysis-sensitive MagSensor (proteolysis-MagSensor). (B) Line plots showing the average phagosome pH as a function of time without and with magnetic force applied. The line curves are averages from 25 (no force) and 20 (with magnetic force) individual phagosomes. Shaded areas represent the SEM. (C) Statistical plots of average acidification rates: 0.48 ± 0.34 pH unit/min (without magnetic manipulation, N = 33) and 0.18 ± 0.20 pH unit/min (with magnetic pulling, N = 26) (D) Statistical plots of average final pH of bead-containing phagosomes: 4.7 ± 0.3 (without magnetic force, N = 33) and 6.3 ± 0.8 (with magnetic force, N = 26). Each box plot indicates the mean (horizontal line) and the interquartile range from 25 to 75% of the corresponding dataset. Statistical significance is highlighted by P values (Student's t test) as follows: \*\*\*\*P < 0.0001 and \*\*\*P < 0.001. (E) Schematic showing the working principle of fluorogenic peptide Z-FR-R110 for phagosome proteolytic activity measurements. (f) Line plots show the average rhodamine 110 intensity (no force, N = 9; with magnetic force, N = 6) indicating proteolysis within bead-containing vacuoles as a function of time with or without magnetic force applied. Shaded areas represent the SEM.

ligand-bound receptors and signaling proteins reorganize spatially to form a phagocytic synapse at the microbe-host cell contact area (1, 3, 64, 65). A key characteristic of this phagocytic synapse is that inhibitory phosphatases like CD45 are spatially excluded from the pathogen-host contact area where activated receptors, such as Dectin-1 and FcyRs, are concentrated (1-3). Based on studies of T cells and B cells (1, 66–68), microscale protein segregation occurring in the phagocytic synapse is likely to be a critical mechanism for sustaining productive signaling from phagocytic receptors, an event preceding the proper assembly of the nascent phagosome. Therefore, we hypothesized that propulsive force exerted during cell entry could affect the formation of the phagocytic synapse formation and thereby trigger a domino effect of disruption to the degradative function of phagosomes that we observed. Because it is unclear which receptors on macrophage cells are responsible for the phagocytosis of *Toxoplasma*, we examined the distribution of the tyrosine phosphatase CD45 at the phagocytic synapse. We labeled CD45 on the live cell membrane using a low concentration of Alexa647 anti-CD45 antibody, following a reported procedure (2). During the internalization of heat-killed *Toxoplasma* without magnetic force, CD45 was excluded from the parasite-cell contact area, as indicated by its lower fluorescence intensity at the contact site compared to that in the surrounding membrane (Fig. 6 A and C and SI Appendix, Fig. S22A). However, when magnetic force was applied, no exclusion of CD45 was observed (Fig. 6  $\emph{B}$  and  $\emph{D}$  and SI Appendix, Fig. S22B). Interestingly, the magnetic force had no effect on the distribution of the cell membrane glycosphingolipid

GM1, which was labeled with CTB-CF488 (SI Appendix, Fig. S23 A and B). Because CD45 has a large, rigid extracellular domain, this suggests that the propulsion force during internalization selectively hindered the reorganization of bulky proteins like CD45 during phagocytic synapse formation (schematic illustration in Fig. 6E). Using Mag-Yeast, we observed that magnetic forces similarly hindered the spatial segregation of CD45 from the GFP labeled Dectin-1 receptor, which binds to the β-glucan on yeast (SI Appendix, Fig. S24). This shows that the force-induced alteration to the phagocytic synapse is not specific to Toxoplasma.

To further test whether the disruption of phagocytic synapse formation was caused by the physical force exerted or by potential biochemical effects of microbial surface components, we examined the phagocytic synapse using magnetic beads coated with IgG for FcγR-mediated phagocytosis (53, 54). Beads of 2.8 μm in diameter were chosen for better quantification of the protein distribution at the synapse (force-distance calibration in SI Appendix, Figs. S25 and S26). We first imaged the distribution of FcyRs by labeling them with a low concentration of F(ab) fragments specific to mouse FcyIII (CD16) and FcyII (CD32) receptors. The F(ab) fragments were fluorescently labeled with CF640R. Without magnetic force, FcγRs clustered at the phagocytic synapse, as indicated by its increased fluorescence intensity (Fig. 7 A and C and SI Appendix, Fig. S27A). The clustering of ligand-bound FcγRs is expected for normal phagocytosis. This also confirmed that labeling the receptors with F(ab) fragments did not block their binding to IgG. In contrast, with magnetic pulling, there was no obvious clustering

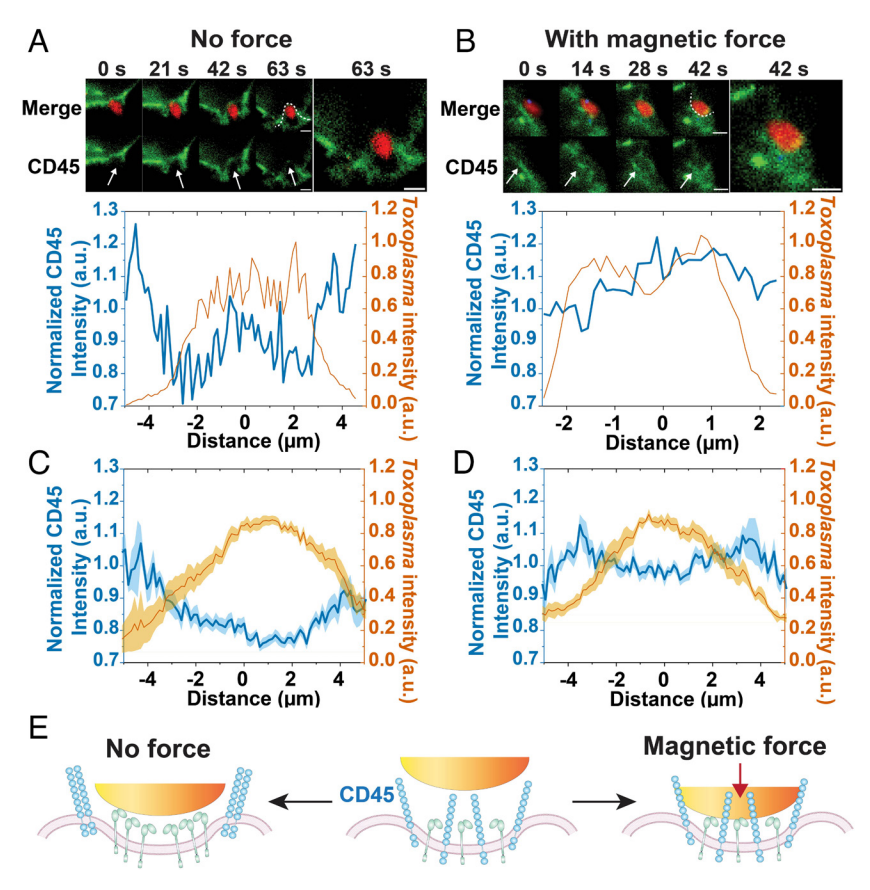


Fig. 6. Propulsive force alters the distribution of phosphatase CD45 at the contact site between a heat-killed Toxoplasma and a RAW 264.7 cell. (A and B) Fluorescence images and line-scan intensity plots showing the distribution of CD45 at the phagocytic synapse, without or with magnetic pulling force. White dotted lines in fluorescence images indicate the line scans along which the fluorescence intensity of CD45 is plotted. The line-scan intensity plots of Toxoplasma are used to indicate the periphery of the cell-parasite contact area. (Scale bars, 2 µm.) (C and D) Average line-scan intensity plots showing the average fluorescence intensity of CD45 at the phagocytic synapse, without or with magnetic pulling force. The line curves are averaged from 18 (no force) and 10 (with magnetic force) single phagosome measurements. Shaded areas represent the SEM. (E) Schematic illustration showing CD45 distribution at the phagocytic synapse without and with magnetic force applied.

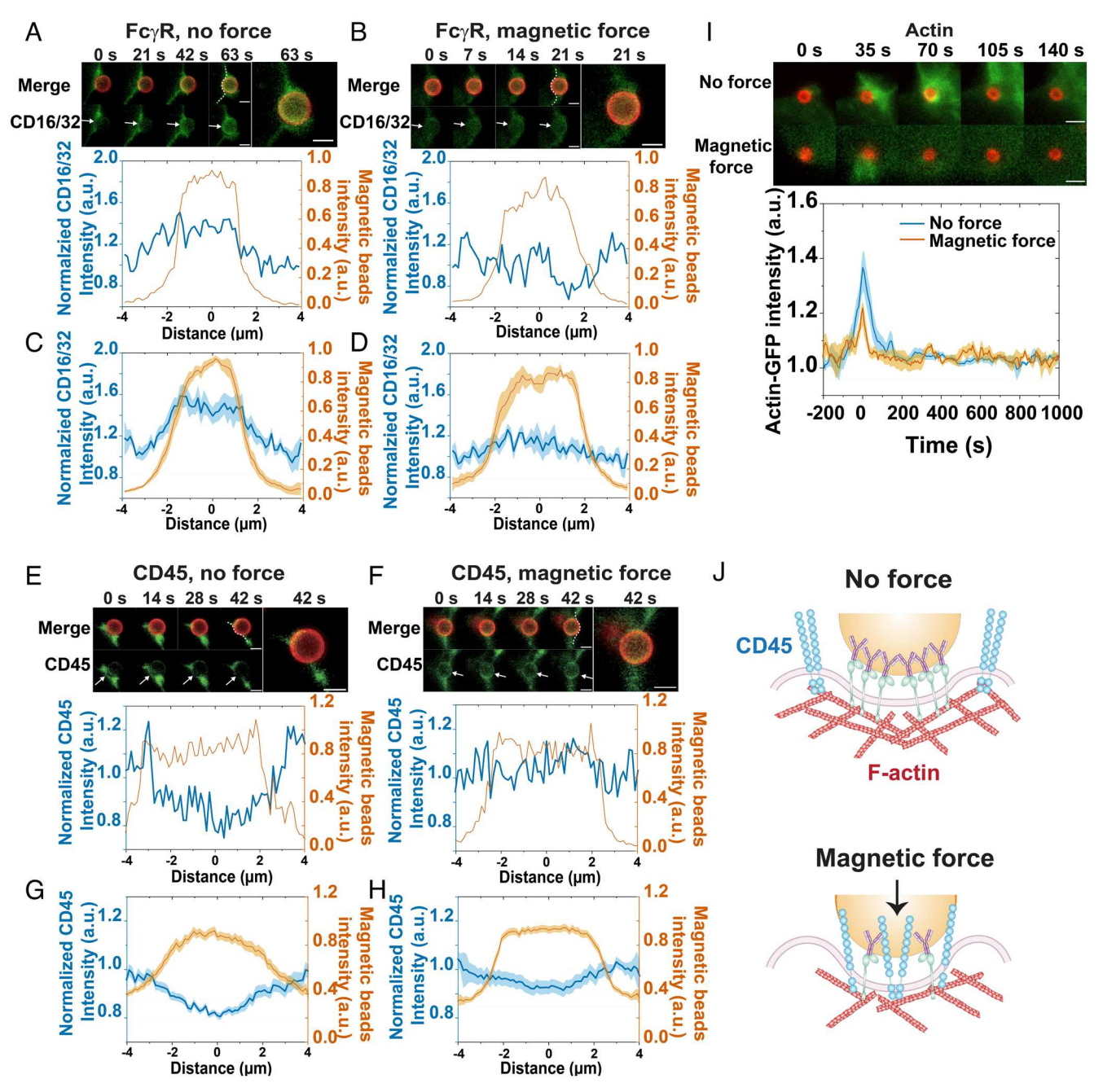


Fig. 7. Propulsive force alters the organization of Fc<sub>γ</sub>Rs (CD16/32), CD45, and actin at the phagocytic synapse. (A-H) Fluorescence images and line-scan intensity plots showing the distribution of Fc<sub>Y</sub>Rs (CD16/32) (A-D) and CD45 (E-H) at the phagocytic synapse during the internalization of IgG opsonized magnetic beads (red), without or with magnetic pulling force. (Scale bars, 2 µm.) White dotted lines in fluorescence images indicate the line scans along which the fluorescence intensity of receptors is plotted. A, B, E, and F are single phagosome data. C, D, G, and H are average line-scan intensity plots showing the average fluorescence intensity of FcγRs (CD16/32) (C and D) and CD45 (G and H) at the phagocytic synapse. Each average line plot is an average of N single phagosome measurements, where N = 10 (C, FcγR no force), 7 (D, FcγR with magnetic force), 30 (G, CD45 no force), and 39 (H, CD 45 with magnetic force). The line-scan intensity plots of magnetic beads are used to indicate the periphery of the cell-bead contact area. Shaded areas represent the SEM. (I) Fluorescence images showing actin (green) during the internalization of opsonized magnetic beads (red). (Scale bars, 2 µm.) Line plots show the average actin-GFP accumulation during phagosome formation as a function of time with no force or without magnetic force. The line curves are averaged from N = 12 (no force) and 13 (with magnetic force) single phagosome measurements. Shaded areas represent the SEM. To align the line plots, time zero is defined at the point when actin intensity reaches the peak value. () Schematic illustrations showing the organization of FcγRs (CD16/32), CD45, and actin, at the phagocytic synapse, without or with magnetic pulling force.

of FcyRs. The fluorescence intensity of FcyRs at the phagocytic synapse remained similar to that in the plasma membrane (Fig. 7 B and D and SI Appendix, Fig. S27B). To test whether FcγRs bound with IgG on the beads, we tried to pull the beads away from the cell surface by reversing the direction of the magnetic force and found that the beads remained bound to the cell. This suggests that the propulsion force at cell entry did not affect the FcyR recognition of ligands, but blocked receptors outside the bead-cell contact site from moving into the contact site to coalescence. Meanwhile, we found that the spatial exclusion of CD45 at the phagocytic synapse was also hindered under magnetic force (Fig. 7 E–H). The consistent observation from using Mag-Toxoplasma, Mag-Yeast, and beads indicates that it is a general phenomenon independent of the specific type of receptors involved.

Activation of FcyRs during phagocytosis is known to trigger polymerization of actin that pushes the membrane protrusion for engulfment (69, 70). Does CD45 remaining in the bead-cell contact site result in reduced signaling from the FcyRs and subsequently reduced remodeling of actin? We confirmed this by imaging the dynamics of actin-GFP during internalization of beads in live cells. As expected for typical phagocytosis, actin rapidly polymerized around nascent phagosomes and then disassembled (Fig. 71 and SI Appendix, Fig. S28A). This peak of actin intensity reportedly coincides with the closure of the phagosome cup (71). However, with applied magnetic force, a significantly reduced amount of actin was observed to polymerize around phagosomes and its presence was more transient (Fig. 71 and SI Appendix, Fig. S28B). Previous studies have noted that the assembly and disassembly of actin around nascent phagosomes tightly controls the maturation of phagosomes, including the recruitment of Rab5 and phagosome fusion with endosomes and lysosomes (72-74). It is therefore plausible that following the propulsive cell entry of a phagocytic target, the physical force hinders the spatial segregation of activated receptors from phosphatases at the phagocytic synapse, leading to reduced signaling from the receptors and thereby reduced remodeling of actin (schematics shown in Fig. 7J). This affects the maturation of nascent phagosomes and diverts them from the canonical phagolysosomal maturation pathway.

Computational Modeling of the Impact of Propulsive Force on the Phagocytic Synapse Formation. We next developed a computational model to understand the mechanism by which propulsion forces impact the organization of receptors and CD45 at the pathogen-cell contact site. We considered apposed regions of the pathogen surface and the macrophage cell surface and implemented a hybrid simulation framework to characterize the spatiotemporal distribution of surface proteins and the shape of the macrophage membrane. The framework utilized a time-dependent Ginzburg-Landau approach to characterize deformations of the macrophage membrane and the Gillespie method to account for protein diffusion and receptor-ligand binding (detail in SI Appendix) (75, 76). In this model, receptors and CD45 were mobile on the macrophage membrane, receptors can bind to immobile ligands on the pathogen surface, and the macrophage membrane can deform in response to a propulsion force exerted by the rigid pathogen surface and the dynamic distribution of surface proteins. An important feature of the model was that a receptor-ligand bond was smaller in size than CD45,

which has a relatively large and rigid extracellular domain. This size difference is the basis of the kinetic segregation model first proposed to understand antigen recognition by T cell receptors (77). To capture the impact of the size difference, we imposed an energy penalty when CD45 was compressed in regions where the surfaces were closer than its natural length (40 nm), or when a receptor-ligand bond was in a region where the distance between surfaces was either larger or smaller than its natural length (15 nm) (78). Mobile surface molecules were more likely to migrate to energetically favorable states than to energetically unfavorable states. In the model, the surface density of CD45 was 54 per µm<sup>2</sup>, based on our experimental estimation of  $54 \pm 14$  CD45 per  $\mu$ m<sup>2</sup> on RAW264.7 cell surfaces (SI Appendix, Fig. S29). The density of FcyR was 325 per µm<sup>2</sup>, estimated based on measurements reported in the literature (79). Other parameters were obtained from the literature or estimated based on measurements in similar systems (SI Appendix, Table S1). We tuned the magnitude of the propulsion force by changing the force constant of a harmonic potential acting on surface elements of the pathogen.

Our simulations revealed that the spatial organization of surface molecules was modulated by the magnitude of the applied force. For small forces (≤7 pN), a central cluster of receptor-ligand bonds formed around the initial cell-pathogen contact site (Fig. 8A and Movie S1). The initial small cluster of receptorligand bonds brought the apposed surfaces to be approximately 15 nm apart, and the cluster grew as unbound receptors diffused into the closely apposed region. This growth continued to drive CD45 molecules to the periphery of the central cluster because of their larger, rigid extracellular domain (\$\approx 40\ nm) (\$\sigma I \text{ Appendix}\$, Fig. S30A). The resulting organization mimics the classic structure of the phagocytic synapse and is consistent with the kinetic segregation model proposed in the context of T cell activation (78). We found that within this weak force regime (≤7 pN), increasing forces promoted faster growth of the receptor-ligand cluster and increased exclusion of CD45, by pushing the apposed cell surfaces closer to facilitate more receptor-ligand binding near the periphery of the central cluster (Fig. 8A and Movies S1 and S2).

Larger applied forces (>7 pN), however, caused a distinctly different organization of surface molecules at the cell-pathogen contact site. The range of forces exerted by motile pathogens and used in our experiments falls within this category. Instead of a single, central cluster of receptor-ligand bonds surrounded by spatially excluded CD45, the contact region was characterized by multiple

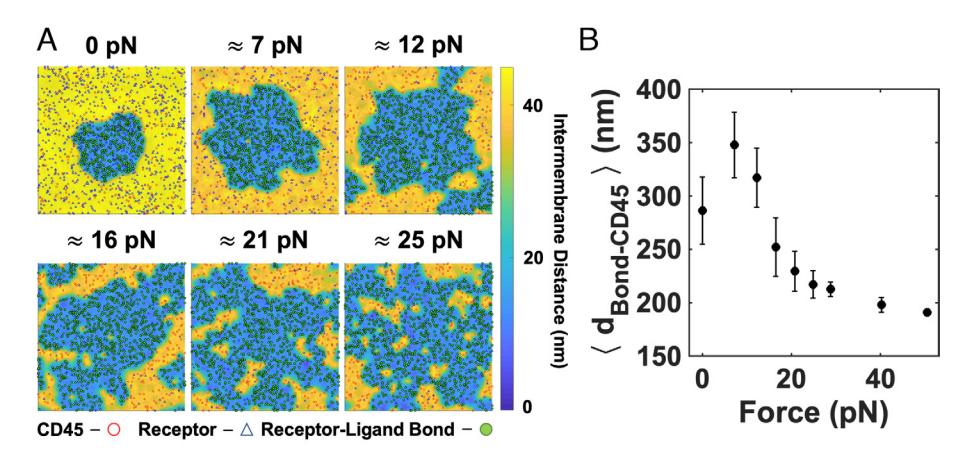


Fig. 8. Applied physical force disrupts protein organization of the early phagocytic synapse in silico. (4) Representative snapshots of simulation trajectories 60 s after initial contact for different magnitudes of applied force. Locations of free receptors (blue triangles), CD45 (red circles), and receptor-ligand bonds (filled green circles) are superimposed on a heat map representing the local distance between the two surfaces. Areas where the distances between the two surfaces are greater than 45 nm are shown in light yellow. Each frame represents a 2 µm × 2 µm patch of membrane. (B) The average distance from each receptor-ligand bond to the nearest CD45 molecule ( $\langle d_{Bond-CD45} \rangle$ ) is plotted as a function of force. Each data point represents the average and SD of 10 independent trajectories.

CD45-rich regions coexisting with dense clusters of receptor-ligand bonds (Fig. 8A). In this large force regime, the applied force rapidly pushed the cell surface and pathogen surface into close contact (Movie S1). This facilitated rapid receptor-ligand binding over a large area extending beyond the initial cluster of bonds (SI Appendix, Fig. S30 A and B). Consequently, CD45-rich domains, owing to their large intermembrane distance (≈40 nm), became trapped within the regions of receptor-ligand bonds that were closely apposed (≈15 nm) (Movie S2). The coexisting regions with different intermembrane distances restrained reorganization into larger domains because of the energetic cost associated with CD45 crossing the closely apposed region of receptor-ligand bonds.

We quantified the extent of spatial exclusion of CD45 from ligand-bound (activated) receptors by calculating the distance from each receptor-ligand bond to the nearest CD45 after 60 s of simulation time (Fig. 8*B*). Within the small force regime (≤7 pN), the spatial separation between the activated receptors and CD45 increased with larger forces (Fig. 8B) and increased with time at each given force (SI Appendix, Fig. S30C). Both results quantitatively support the observations that the ligand-bound receptors formed a central cluster with CD45 excluded to the periphery and that larger forces within this weak force regime caused faster growth of the receptor cluster. Within the large force regime (>7 pN), the average distance between each ligand-bound receptor and its nearest CD45 was significantly reduced compared to the small force regime, and it decreased with increasing force. This is consistent with the observation of altered surface organization, where multiple CD45-rich domains remained immersed with clusters of receptor-ligand bonds. The time dependence of the average distance (SI Appendix, Fig. S30C) showed the rapid formation of coexisting domains of activated receptors and CD45, which then slowly coalesced.

We further found that the biphasic force-dependence of the synapse formation was not affected by the surface density of receptors or CD45 (SI Appendix, Figs. S31 and S32). However, the threshold force needed to hinder the protein segregation was not affected by receptor density but changed with CD45 density. With increasing surface density of CD45, larger forces were required to overcome the energy penalty to bring the two surfaces close enough for receptor binding in the peripheral region. In the large force regime, we also examined the effect of force duration, and found that transient application of the force for 10 s or longer hindered the phagocytic synapse assembly to the same extent as persistent forces (SI Appendix, Fig. S33).

Taken together, the simulation results demonstrate that applied force can lead to the reorganization of the surface molecules that control downstream signaling. The smaller distance between the phosphatase CD45 and activated receptors at larger forces plausibly explains our experimental observations of reduced receptor phosphorylation and signaling under magnetic force.

#### **Discussion**

In this study, we demonstrate how the physical process of propulsive cell entry by motile pathogens redirects the intracellular trafficking of internalized pathogens away from the degradation pathway. This study was motivated by emerging evidence that pathogen motility plays important roles in their invasion of the host. However, how this physical process affects the pathogen-host interaction remains unclear. The major challenge is to differentiate the physical effect of motile pathogens from the biochemical effect of the associated virulence factors. To overcome this challenge, we used external magnetic force fields to induce propulsive cell entry similar to motile pathogens. This approach allowed us to elucidate the mechanism by which physical forces, distinct from the effect of virulence factors, contribute to modulating the intracellular trafficking fate of pathogens. We confirmed our findings using Toxoplasma, yeast cells, and opsonized beads as phagocytic targets.

A key finding of this study is that physical forces during cell entry alter protein spatial organization at the phagocytic synapse. This serves as a decision-making point where internalized pathogens are redirected into vacuoles that fail to mature into degradative units. Our experiments and simulations demonstrate that large propulsion forces hinder the spatial exclusion of the bulky phosphatase CD45 from activated receptors, limiting productive signaling. Previous studies have highlighted the importance of spatial segregation of receptors from phosphatases in sustaining the activation of receptors (1–3) and promoting phagocytosis (2). Our results reveal that the phagocytic synapse plays a crucial role beyond regulating receptor signaling; it also determines the intracellular trafficking fate of phagosomes in two plausible ways. First, the phagocytic synapse becomes part of a nascent phagosome, influencing its membrane composition. The altered membrane biology can then affect phagosome recruitment of signaling proteins and fusion with lysosomes, and thereby the degradative fate. Second, receptor activation at the synapse triggers downstream signaling events, including actin remodeling, which affects the recruitment of the endocytic marker Rab5 and fusion with lysosomes (72-74, 80). In support of this idea, we observed that hindering phosphatase CD45 exclusion by large forces reduced actin assembly around nascent phagosomes, resulting in decreased recruitment of necessary signaling proteins for phagosome maturation.

Prior studies have not explored the impact of physical forces on phagocytic synapse formation. We revealed a mechanism based on the kinetic segregation model (78), which considers the force effect on the energetic landscape shaped by size differences between ligand-bound receptors and phosphatase CD45. However, beyond this model, the applied physical forces may affect the phagocytic synapse and phagosome functions through other mechanisms, such as increased membrane tension, which was shown to influence endocytosis (81).

In addition to the force-induced alteration of the phagocytic synapse, we made a surprising observation: inactive parasites were degraded in phagolysosomes, while the same inactive parasites propelled by magnetic force during internalization entered an alternative nondegradative intracellular trafficking pathway. Our results suggest a model where force-induced protein reorganization disrupts the canonical maturation of nascent vacuoles into degradative phagolysosomes. This disruption affects the assembly of endocytic markers (Rab5, Rab7, and LAMP1) on parasite-residing vacuoles, preventing their fusion with endosomes and lysosomes. Consequently, the vacuoles cannot acquire the hydrolytic enzymes and ATPases needed for content digestion and continuous vacuole lumen acidification. Our findings emphasize the tight regulation of phagosome maturation and the critical role of cell entry in determining the fate of internalized cargos. It's worth noting that the observed disruptive effects may not solely result from the organization of receptors and CD45 in the synapse; other membrane proteins involved in phagocytic synapse formation could also be affected by applied force. Additionally, propulsion forces may also impact lipid biology of the vacuole. The canonical phagosome maturation pathway entails crucial steps, such as lipid exchange and lipid hydrolysis (82, 83). Therefore, lipids may play a pivotal role in mediating the effect of forces exerted at the pathogen-host contact area to influence the phagosome maturation. Our findings present open questions for future research.

We used Toxoplasma as a model pathogen (29–31) and extended our findings to yeast cells and opsonized beads to confirm that force-induced disruption of pathogen degradation is a general phenomenon. It suggests that motile pathogens can use physical forces during invasion to evade immune degradation. This doesn't contradict the established evidence that pathogens use virulent factors to perturb phagosome maturation for evading degradation (16–19). Rather, our results suggest that the physical effect of pathogen motility can enhance the biochemical effect of virulence factors, and it's plausible that a single pathogen employs multiple evasion mechanisms. Unlike previous studies focusing on pathogen motility for binding and penetration into host cells, our research sheds light on how pathogen motility affects their intracellular fate after cell entry. Intriguingly, our computer simulations showed that the impact of applied forces depends on their magnitude. Large forces hinder protein segregation at the phagocytic synapse, while small forces can have the opposite effect. This suggests that certain pathogens may become more vulnerable to immune degradation if the generated force is small. This underscores the prospect of targeting pathogen movement as a strategy to combat intracellular pathogens.

## **Materials and Methods**

Details of reagents, cells, and experimental methods are provided in *SI Appendix*.

Fabrication of Mag-Toxoplasma and Other Sensors. Heat-killed Toxoplasma tachyzoites were first conjugated with 200-nm magnetic nanoparticles via EDC reaction and then with pH-sensitive dye pHrodo Red. To prepare FRET-MagSensors for the fusion assay, streptavidin labeled with the FRET donor Alexa 568 was conjugated on 1-µm Dynabeads. To fabricate pH-MagSensors, Dynabeads with various sizes were conjugated with streptavidin labeled with either pHrodoRed or reference dye CF640R. Proteolysis-MagSensors were prepared by labeling 1-µm Dynabeads with streptavidin-CF640R and Z-FR-R110 peptide.

Live Cell Fluorescence Imaging. Imaging was done on a Nikon Eclipse-Ti inverted microscope equipped with a 1.49 N.A. ×100 TIRF objective and an Andor iXon3 EMCCD camera. In FRET-fusion assays, lysosomes were labelled by

- H. S. Goodridge et al., Activation of the innate immune receptor Dectin-1 upon formation of a "phagocytic synapse". Nature 472, 471-475 (2011).
- M. H. Bakalar et al., Size-dependent segregation controls macrophage phagocytosis of antibodyopsonized targets. Cell 174, 131-142.e13 (2018).
- S. A. Freeman et al., Integrins form an expanding diffusional barrier that coordinates phagocytosis. Cell 164, 128-140 (2016).
- B. Steinberg, K. Huynh, S. Grinstein, Phagosomal Acidification: Measurement, Manipulation and Functional Consequences (Portland Press Ltd., 2007).
- S. Duclos *et al.*, Rab5 regulates the kiss and run fusion between phagosomes and endosomes and the acquisition of phagosome leishmanicidal properties in RAW 264.7 macrophages. *J. Cell Sci.* 113, 3531-3541 (2000).
- M. C. Kielian, Z. A. Cohn, Phagosome-lysosome fusion-Characterization of intracellular membranefusion in mouse macrophages. J. Cell Biol. 85, 754–765 (1980).
- V. Claus et al., Lysosomal enzyme trafficking between phagosomes, endosomes, and lysosomes in J774 macrophages-Enrichment of cathepsin H in early endosomes. J. Biol. Chem. 273, 9842-9851
- R. M. Yates, A. Hermetter, D. G. Russell, The kinetics of phagosome maturation as a function of phagosome/lysosome fusion and acquisition of hydrolytic activity. Traffic 6, 413-420 (2005).
- A. M. Lennon-Dumenil et al., Analysis of protease activity in live antigen-presenting cells shows regulation of the phagosomal proteolytic contents during dendritic cell activation. J. Exp. Med. 196, 529-540 (2002).
- 10. C. Persson et al., Cell-surface-bound Yersinia translocate the protein tyrosine phosphatase YopH by a polarized mechanism into the target cell. Mol. Microbiol. 18, 135-150 (1995).
- 11. S. Håkansson, E. E. Galyov, R. Rosqvist, H. Wolf-Watz, The Yersinia YpkA Ser/Thr kinase is translocated and subsequently targeted to the inner surface of the HeLa cell plasma membrane. Mol. Microbiol. 20, 593-603 (1996).
- 12. E. Frithz-Lindsten, Y. Du, R. Rosqvist, Å. Forsberg, Intracellular targeting of exoenzyme S of Pseudomonas aeruginosa via type III-dependent translocation induces phagocytosis resistance, cytotoxicity and disruption of actin microfilaments. Mol. Microbiol. 25, 1125-1139 (1997).
- L. Garrity-Ryan et al., The arginine finger domain of ExoT contributes to actin cytoskeleton disruption and inhibition of internalization of Pseudomonas aeruginosa by epithelial cells and macrophages. Infect. Immun. 68, 7100-7113 (2000).

incubating macrophage cells with biotin-BSA-Alexa 647 in full DMEM overnight followed by a 2-h chasing period.

Magnetic Tweezers Setup. A magnetic tweezers setup was mounted on a Nikon Eclipse-Ti inverted microscope. The magnetic solenoid had a tip of  $\approx 1 \,\mu m$ (diameter), and its position was controlled using a micromanipulator.

Image Analysis. The fluorescence intensity of phagosome sensors, actin, and endocytic was analyzed using MATLAB as described previously (58). Distribution of FcyRs and CD45 at the phagocytic synapse was analyzed using Image J.

Simulation. A computational framework was developed with the pathogen surface positioned near a part of the macrophage surface. Surface proteins were represented as diffusive particles; receptors on the macrophage surface can bind to immobile ligands on the pathogen surface reversibly. Dynamics of the particles were governed by a stochastic reaction-diffusion process. The membrane shape was characterized by a time-dependent Ginzburg-Landau model.

Data, Materials, and Software Availability. All study data are included in the manuscript and/or supporting information. Raw data used to generate main figures and source code for simulation have been deposited at https://doi. org/10.6084/m9.figshare.22655089.v1 (84).

ACKNOWLEDGMENTS. We thank Dr. Ke Hu and Dr. John Murray at Arizona State University for providing Toxoplasma strains and insightful discussion; Dr. Sergio Grinstein at The Hospital for Sick Children Research Institute (Canada) for providing plasmids of endocytic markers and insightful discussion; Dr. Jun Yan at University of Louisville for providing the green fluorescent protein (GFP)-Dectin-1 expressing RAW264.7 cells; and Dr. John Choy at the Catholic University of America for providing the yeast strain. We thank the following staff members at Indiana University: Andrew Alexander at the Electronic Instrument Services, Dr. Yi Yi at the Nanoscale Characterization Center, and Dr. Giovanni Gonzalez-Gutierrez at the Physical Biochemistry Instrumentation Facility. This work was supported by the National Institute Of General Medical Sciences of the National Institutes of Health (NIH) under Award Number R35GM124918 (to Y.Y.) and the National Science Foundation under Award Number PHY1753017 (to S.M.A.). The content is solely the responsibility of the authors and does not necessarily represent the official views of the NIH.

Author affiliations: aDepartment of Chemistry, Indiana University, Bloomington, IN 47405-7102; and <sup>b</sup>Department of Chemical and Biomolecular Engineering, University of Tennessee, Knoxville, TN 37996

- 14. B. F. Hall, P. Webster, A. K. Ma, K. A. Joiner, N. W. Andrews, Desialylation of lysosomal membrane glycoproteins by Trypanosoma cruzi: A role for the surface neuraminidase in facilitating parasite entry into the host cell cytoplasm. J. Exp. Med. 176, 313-325 (1992).
- 15. M. J. McConville, S. J. Turco, M. Ferguson, D. L. Sacks, Developmental modification of lipophosphoglycan during the differentiation of Leishmania major promastigotes to an infectious stage. EMBO J. 11, 3593-3600 (1992).
- D. Wong, H. Bach, J. Sun, Z. Hmama, Y. Av-Gay, Mycobacterium tuberculosis protein tyrosine phosphatase (PtpA) excludes host vacuolar-H+-ATPase to inhibit phagosome acidification. Proc. Natl. Acad. Sci. U.S.A. 108, 19371–19376 (2011).
- 17. A. Mehra et al., Mycobacterium tuberculosis Type VII secreted effector EsxH targets host ESCRT to impair trafficking. PLoS Pathog. 9, e1003734 (2013).
- 18. E. Hertzén et al., M1 protein-dependent intracellular trafficking promotes persistence and replication of Streptococcus pyogenes in macrophages. J. Innate Immun. 2, 534-545 (2010).
- A. Gallois, J. R. Klein, L.-A. Allen, B. D. Jones, W. M. Nauseef, Salmonella pathogenicity island 2-encoded type III secretion system mediates exclusion of NADPH oxidase assembly from the phagosomal membrane. J. Immunol. 166, 5741-5748 (2001).
- C. Josenhans, S. Suerbaum, The role of motility as a virulence factor in bacteria. Int. J. Med. Microbiol. 291, 605-614 (2002).
- D. Sacks, A. Sher, Evasion of innate immunity by parasitic protozoa. *Nat. Immunol.* **3**, 1041–1047 (2002). C. Dietrich, K. Heuner, B. C. Brand, J. Hacker, M. Steinert, Flagellum of Legionella pneumophila
- positively affects the early phase of infection of eukaryotic host cells. Infect. Immun. 69, 2116-2122 (2001)
- 23. D. Soldati, B. J. Foth, A. F. Cowman, Molecular and functional aspects of parasite invasion. *Trends* Parasitol. 20, 567-574 (2004).
- M. B. Heintzelman, Gliding motility in apicomplexan parasites. Semin. Cell Dev. Biol. 46, 135-142 (2015).
- K. Frenal, J. F. Dubremetz, M. Lebrun, D. Soldati-Favre, Gliding motility powers invasion and egress in Apicomplexa. Nat. Rev. Microbiol. 15, 645-660 (2017).
- M. M. Shimogawa et al., Parasite motility is critical for virulence of African trypanosomes. Sci. Rep. 8, 9122 (2018).
- 27. J. M. Dobrowolski, V. B. Carruthers, L. D. Sibley, Participation of myosin in gliding motility and host cell invasion by Toxoplasma gondii. Mol. Microbiol. 26, 163-173 (1997).

- 28. J. A. Whitelaw et al., Surface attachment, promoted by the actomyosin system of Toxoplasma gondii is important for efficient gliding motility and invasion. BMC Biol. 15, 1 (2017).
- D. G. Mordue, N. Desai, M. Dustin, L. D. Sibley, Invasion by Toxoplasma gondii establishes a moving junction that selectively excludes host cell plasma membrane proteins on the basis of their membrane anchoring. J. Exp. Med. 190, 1783-1792 (1999).
- L. D. Sibley, Intracellular parasite invasion strategies. Science 304, 248-253 (2004).
- J. M. Dobrowolski, L. D. Sibley, Toxoplasma invasion of mammalian cells is powered by the actin cytoskeleton of the parasite. Cell 84, 933-939 (1996).
- L. D. Sibley, E. Weidner, J. L. Krahenbuhl, Phagosome acidification blocked by intracellular Toxoplasma-gondii. Nature 315, 416-419 (1985).
- K. A. Joiner, S. A. Fuhrman, H. M. Miettinen, L. H. Kasper, I. Mellman, Toxoplasma-gondii-Fusion competence of parasitophorous vacuoles in Fc-receptor transfected fibroblasts. Science 249, 641-646 (1990).
- 34. D. G. Mordue, S. Hakansson, I. Niesman, L. D. Sibley, Toxoplasma gondii resides in a vacuole that avoids fusion with host cell endocytic and exocytic vesicular trafficking pathways. Exp. Parasitol. 92,
- I. Coppens et al., Toxoplasma gondii sequesters lysosomes from mammalian hosts in the vacuolar space. Cell 125, 261-274 (2006).
- D. G. Mordue, L. D. Sibley, Intracellular fate of vacuoles containing Toxoplasma gondii is determined at the time of formation and depends on the mechanism of entry. J. Immunol. 159, 4452-4459
- B. A. Butcher, E. Y. Denkers, Mechanism of entry determines the ability of Toxoplasma gondii to inhibit macrophage proinflammatory cytokine production. Infect. Immun. 70, 5216-5224 (2002).
- N. K. Kisalu, G. Langousis, L. A. Bentolila, K. S. Ralston, K. L. Hill, Mouse infection and pathogenesis by Trypanosoma brucei motility mutants. Cell. Microbiol. 16, 912-924 (2014).
- P. Cossart, A. Helenius, Endocytosis of viruses and bacteria. *Cold Spring Harb. Perspect. Biol.* **6**, a016972 (2014).
- A. M. Pauwels, M. Trost, R. Beyaert, E. Hoffmann, Patterns, receptors, and signals: Regulation of phagosome maturation. *Trends Immunol.* **38**, 407–422 (2017).
- A. Jahraus et al., In vitro fusion of phagosomes with different endocytic organelles from J774 macrophages. J. Biol. Chem. 273, 30379-30390 (1998).
- M. Desjardins, N. N. Nzala, R. Corsini, C. Rondeau, Maturation of phagosomes is accompanied by changes in their fusion properties and size-selective acquisition of solute materials from endosomes. J. Cell Sci. 110, 2303-2314 (1997).
- K. K. Huynh et al., LAMP proteins are required for fusion of lysosomes with phagosomes. EMBO J. 26, 313-324 (2007)
- H. J. Ullrich, W. L. Beatty, D. G. Russell, Direct delivery of procathepsin D to phagosomes: Implications for phagosome biogenesis and parasitism by Mycobacterium. *Eur. J. Cell Biol.* **78**, 739-748 (1999).
- Y. K. Oh et al., Rapid and complete fusion of macrophage lysosomes with phagosomes containing Salmonella typhimurium. *Infect. Immun.* 64, 3877–3883 (1996).
- R. Garcia-Rodas, F. Gonzalez-Camacho, J. L. Rodriguez-Tudela, M. Cuenca-Estrella, O. Zaragoza, The interaction between Candida Krusei and murine macrophages results in multiple outcomes, including intracellular survival and escape from killing. Infect. Immun. 79, 2136-2144 (2011).
- 47. C. Zahn et al., Measurement of the magnetic moment of single Magnetospirillum gryphiswaldense cells by magnetic tweezers. Sci. Rep. 7, 3558 (2017).
- A. R. Bausch, W. Moller, E. Sackmann, Measurement of local viscoelasticity and forces in living cells by magnetic tweezers. Biophys. J. 76, 573-579 (1999).
- P. Kollmannsberger, B. Fabry, High-force magnetic tweezers with force feedback for biological applications. Rev. Sci. Instrum. 78, 114301 (2007).
- C. Jiang, T. A. Lionberger, D. M. Wiener, E. Meyhofer, Electromagnetic tweezers with independent force and torque control. Rev. Sci. Instrum. 87, 084304 (2016).
- R. V. Stadler, L. A. White, K. Hu, B. P. Helmke, W. H. Guilford, Direct measurement of cortical force generation and polarization in a living parasite. Mol. Biol. Cell 28, 1912-1923 (2017).
- M. Mizutani, Y. Sasajima, M. Miyata, Force and stepwise movements of gliding motility in human pathogenic bacterium Mycoplasma pneumoniae. Front. Microbiol. 12, 747905 (2021).
- K. Newton, V. M. Dixit, Signaling in innate immunity and inflammation. Cold Spring Harb. Perspect. Biol. 4, a006049 (2012).
- Leukoc. Biol. 72, 1092-1108 (2002).
- Y. Yu, Z. Zhang, G. F. W. Walpole, Y. Yu, Kinetics of phagosome maturation is coupled to their intracellular motility. Commun. Biol. 5, 1014 (2022).

- 56. G. L. Lukacs, O. D. Rotstein, S. Grinstein, Phagosomal acidification is mediated by a vacuolar-type H+-ATPase in murine macrophages. J. Biol. Chem. 265, 21099-21107 (1990).
- G. H. Sun-Wada, H. Tabata, N. Kawamura, M. Aoyama, Y. Wada, Direct recruitment of H+-ATPase from lysosomes for phagosomal acidification. J. Cell Sci. 122, 2504-2513 (2009).
- B. E. Steinberg, K. K. Huynh, S. Grinstein, Phagosomal acidification: Measurement, manipulation and functional consequences. Biochem. Soc. Trans. 35, 1083-1087 (2007).
- S. Lee, Z. Zhang, Y. Yu, Real-time simultaneous imaging of acidification and proteolysis in single phagosomes using bifunctional janus particle probes. Angew. Chem. Int. Ed. Engl. 60, 26734-26739 (2021), 10.1002/anie.202111094.
- A. Savina et al., NOX2 controls phagosomal pH to regulate antigen processing during crosspresentation by dendritic cells. *Cell* **126**, 205-218 (2006).
- C. G. Zou, Y. C. Ma, L. L. Dai, K. Q. Zhang, Autophagy protects C. elegans against necrosis during Pseudomonas aeruginosa infection. *Proc. Natl. Acad. Sci. U.S.A.* **111**, 12480–12485 (2014).
- C. J. Luke et al., An intracellular serpin regulates necrosis by inhibiting the induction and sequelae of lysosomal injury. Cell 130, 1108-1119 (2007).
- P. L. McNeil, L. Tanasugarn, J. B. Meigs, D. L. Taylor, Acidification of phagosomes is initiated before lysosomal enzyme activity is detected. J. Cell Biol. 97, 692-702 (1983).
- R. K. Tsai, D. E. Discher, Inhibition of "self" engulfment through deactivation of myosin-II at the phagocytic synapse between human cells. J. Cell Biol. 180, 989-1003 (2008).
- M. S. Itano et al., Super-resolution imaging of C-type lectin spatial rearrangement within the dendritic cell plasma membrane at fungal microbe contact sites. Front. Phys. 2, 46 (2014).
- E. D. C. Mcfarland et al., Correlation between Src family member regulation by the protein-tyrosinephosphatase Cd45 and transmembrane signaling through the T-cell receptor. Proc. Natl. Acad. Sci. U.S.A. **90**, 1402–1406 (1993).
- P. Shrivastava, T. Katagiri, M. Ogimoto, K. Mizuno, H. Yakura, Dynamic regulation of Src-family kinases by CD45 in B cells. *Blood* **103**, 1425–1432 (2004).

  M. L. Hermiston, J. Zikherman, J. W. Zhu, CD45, CD148, and Lyp/Pep: Critical phosphatases
- regulating Src family kinase signaling networks in immune cells (vol 228, pg 288, 2009). Immunol. Rev. 229, 387-387 (2009).
- H. Park, D. Cox, Cdc42 regulates Fc(gamma) receptor-mediated phagocytosis through the activation and phosphorylation of Wiskott-Aldrich Syndrome Protein (WASP) and neural-WASP. Mol. Biol. Cell 20, 4500-4508 (2009).
- S. A. Freeman, S. Grinstein, Phagocytosis: Receptors, signal integration, and the cytoskeleton. Immunol. Rev. 262, 193-215 (2014).
- C. C. Scott et al., Phosphatidylinositol-4,5-bisphosphate hydrolysis directs actin remodeling during phagocytosis. J. Cell Biol. 169, 139-149 (2005).
- I. Guérin, C. de Chastellier, Disruption of the actin filament network affects delivery of endocytic contents marker to phagosomes with early endosome characteristics: The case of phagosomes with pathogenic mycobacteria. Eur. J. Cell Biol. 79, 735–749 (2000).
- M. Kitano, M. Nakaya, T. Nakamura, S. Nagata, M. Matsuda, Imaging of Rab5 activity identifies essential regulators for phagosome maturation. Nature 453, 241-245 (2008).
- Y. Yu, Z. Zhang, Y. Yu, Timing of phagosome maturation depends on their transport switching from actin to microtubule tracks. *J. Phys. Chem. B* **127**, 9312–9322 (2023).
- D. T. Gillespie, Stochastic simulation of chemical kinetics. Annu. Rev. Phys. Chem. 58, 35–55 (2007).
- S. Raychaudhuri, A. K. Chakraborty, M. Kardar, Effective membrane model of the immunological synapse. Phys. Rev. Lett. 91, 208101 (2003).
- S. J. Davis, P. A. van der Merwe, The kinetic-segregation model: TCR triggering and beyond. Nat. Immunol. 7, 803-809 (2006).
- R. H. Pullen, S. M. Abel, Catch bonds at T cell interfaces: Impact of surface reorganization and membrane fluctuations. Biophys. J. 113, 120-131 (2017).
- F. Krombach et al., Cell size of alveolar macrophages: An interspecies comparison. Environ. Health Persp. 105, 1261-1263 (1997).
- D. Liebl, G. Griffiths, Transient assembly of F-actin by phagosomes delays phagosome fusion with lysosomes in cargo-overloaded macrophages. J. Cell Sci. 122, 2935–2945 (2009).
- U. Djakbarova, Y. Madraki, E. T. Chan, C. Kural, Dynamic interplay between cell membrane tension and clathrin-mediated endocytosis. *Biol. Cell* **113**, 344–373 (2021).
  F. Hullin-Matsuda, T. Taguchi, P. Greimel, T. Kobayashi, Lipid compartmentalization in the endosome
- system. Semin. Cell Dev. Biol. **31**, 48–56 (2014).
- S. Arumugam, A. Kaur, The lipids of the early endosomes: Making multimodality work. Chembiochem 18, 1053-1060 (2017).
- Z. Zhang et al., Simulation source code and raw data used to generate main figures. Figshare. https://doi.org/10.6084/m9.figshare.22655089.v1. Deposited 23 April 2023.